Random Surface Discretizations and the Renormalization of the Bending Rigidity

G. Gompper, D. Kroll

J. Phys. I France **6** (1996) 1305–1320 OCTOBER **1996**, PAGE 1305

Random Surface Discretizations and the Renormalization of the Bending Rigidity

G. Gompper ([1,2,*]) and D.M. Kroll ([3])

([1]) Max-Planck-Institut für Kolloid- und Grenzflächenforschung, Kantstrasse 55, 14513 Teltow, Germany
([2]) Sektion Physik der Ludwig-Maximilians-Universität München, Theresienstrasse 37, 80333 München, Germany
([3]) Department of Medicinal Chemistry, and Minnesota Supercomputer Institute, University of Minnesota, 308 Harvard Street SE, Minneapolis, MN 55455, USA

(Received 15 March 1996, accepted 12 June 1996)

PACS.05.40.+j – Fluctuation phenomena, random processes, and Brownian motion
PACS.64.60.Fr – Equilibrium properties near critical points, critical exponents
PACS.87.22.Bt – Membrane and subcellular physics and structure

Abstract. — The effect of thermal fluctuations on the properties of fluid vesicles is studied using Monte Carlo simulations and scaling arguments. It is shown that the commonly used discretization of the bending energy on triangulated surfaces — which is based on the squared difference of unit normal vectors of neighboring triangles — is problematic because the relation between the coupling constant λ and the bending rigidity κ is shape dependent (in the limit $\lambda \to \infty$). In contrast, discretizations based on the square of local averages of the mean curvature do not share this problem. Nevertheless, the scaling behavior of spherical vesicles is found to be unaffected by this deficiency of the former discretization. An explicit calculation of the average volume $\langle V \rangle$ in the large-κ limit reveals that $\langle V \rangle$ is not a homogeneous function of the persistence length ξ_p and the vesicle radius, but that there is a weak breakdown of scaling, with a logarithmic correction term of the form $\ln(4\pi\kappa/3)$. Monte Carlo data obtained using both discretizations are consistent with this prediction and provide clear evidence for a κ-dependence of the persistence length of the form $\xi_p \sim \exp[4\pi\kappa/3]$, in agreement with field-theoretic renormalization group results.

1. Introduction

The thermal behavior of fluid membranes — flexible, parametrization invariant surfaces of constant area — has attracted a great deal of attention recently [1, 2]. The structure and behavior of many complex systems in biology, chemistry, and physics can be described in terms of the elasticity and fluctuations of their constituent membranes. Two examples are the cell membranes of mammalian red blood cells and the interfaces between oil and water in microemulsions. In many of these cases the surface tension is either very small or vanishes identically, so that the form and fluctuations of these surfaces are controlled by their elastic bending energy. For membranes which do not have a preferred radius of curvature, the

(*) Author for correspondence (e-mail: gompper@rigel.mpikg-teltow.mpg.de)

curvature elastic energy has the form [3,4]

$$\beta\mathcal{H} = \int \mathrm{d}S \left[\frac{1}{2}\kappa H^2 + \bar{\kappa}K\right] , \tag{1}$$

where κ is the bending rigidity, $\bar{\kappa}$ the saddle-splay modulus (both measured in units of $k_{\mathrm{B}}T$), and H and K are the trace and the determinant of the curvature tensor (or twice the mean and the Gaussian curvature), respectively. For a connected surface, the integral of the Gaussian curvature is related, by the Gauss-Bonnet theorem $\int \mathrm{d}S\ K = 4\pi(1-g)$, to the genus g, or number of handles, of the surface. For fixed topology, the second term in equation (1) therefore gives a constant contribution to the free energy.

The free-energy cost of imposing a deformation of length scale ℓ can be described in terms of a scale-dependent renormalized bending rigidity $\kappa(\ell)$. Recent calculations [5–7] have shown that $\kappa(\ell)$ is softened by fluctuations, and decreases as

$$\kappa(\ell) = \kappa - \frac{3}{4\pi}\ln(\ell/a_0) \tag{2}$$

to leading order in $1/\kappa$, where a_0 is a microscopic cutoff length. Most authors agree on the value $3/(4\pi)$ of the prefactor of the logarithm in equation (2); a notable exception is Helfrich [8], who predicts $1/(4\pi)$. The length scale at which $\kappa(\ell)$ vanishes is the persistence length, $\xi_{\mathrm{p}} \sim a_0 \exp[4\pi\kappa/3]$, beyond which the orientations of distant points on a membrane become uncorrelated. Recent Monte Carlo simulations [9] have provided strong evidence that (2) is indeed correct. Furthermore, these simulations clearly show that for a fixed topology, there is no phase transition for finite κ so that for large enough membrane size and fixed κ, membranes are always crumpled. The crumpled state of self-avoiding membranes is a collapsed, ramified structure characterized by branched polymer scaling behavior [10–13]. The thermodynamic consequences of the softening of the bending rigidity (as well as the thermal stiffening of the saddle-splay modulus $\bar{\kappa}$) is an active area of research [14–16], and many questions remain open.

A detailed understanding of the scale dependence of the bending rigidities is crucial if one is to fully appreciate the consequences of phenomenological models of membrane phase behavior. A quantitative analysis of the model requires, in particular, the correct measure [17], equivalence classes, and operator discretizations on random surfaces. Whereas analytical studies of the model are possible in the large bending rigidity regime, simulation studies of triangulated random surfaces are the only method currently available for determining the behavior in the crucial fluctuation dominated regime $\kappa, \bar{\kappa} \sim 1$. In this paper, we return to the question of operator discretizations on random surfaces and the renormalization of the bending rigidity. In Section 2 we show that the commonly used expression [18]

$$\beta\mathcal{H}_{\mathrm{d}}^{\mathrm{nn}} = \lambda \sum_{\langle\alpha,\beta\rangle} (1 - \mathbf{n}_\alpha \cdot \mathbf{n}_\beta) \tag{3}$$

for the bending energy of a triangulated surface, where $\mathbf{n}_\alpha$ is the unit normal vector of triangle α, and the sum runs over all pairs of neighboring triangles, is deficient because the relation between the rigidity constant λ and κ in equation (1) depends on the shape of the surface. In contrast, it is shown that discretizations based on the square of local averages of the mean curvature do not share this problem. One acceptable choice is a discretization of the Laplacian-squared representation of the bending energy,

$$\int \mathrm{d}S\ (\Delta\mathbf{R})^2 \equiv \int \mathrm{d}S\ H^2 , \tag{4}$$

where $\mathbf{R}$ is the coordinate vector of the surface element in the three-dimensional embedding space, and Δ is the covariant Laplacian, described by Itzykson in reference [19]. Other choices, such as those used in references [20,21], are equally acceptable. In Section 3, we analyze Monte Carlo data for the average volume $\langle V \rangle$ of flaccid fluid vesicles using the scaling ansatz

$$\langle V \rangle \sim N^{3/2} \Theta(\sqrt{N}/\xi_{\mathrm{p}}), \tag{5}$$

where N is the number of surface monomers and ξ_{p} is the persistence length. Data previously presented in reference [9] obtained using the bending energy (3) and measure

$$\prod_i \mathrm{d}\mathbf{R}_i (q_i/3)^{3/2} , \tag{6}$$

where $\mathbf{R}_i$ is the coordinate vector of vertex i and q_i its coordination number, are included in our analysis. New results obtained using bending energy (3) and the naive measure

$$\prod_i \mathrm{d}\mathbf{R}_i \tag{7}$$

are also presented, and it is shown that the scaling behavior, and in particular, the behavior of the renormalized bending rigidity, is not affected by the choice of measure. A simple argument is also given which indicates that the differences between these two measures is indeed irrelevant in the renormalization-group sense. Finally, results obtained using a discretization of the Laplacian-squared representation (4) of the bending energy and naive measure (7) are analyzed. It is shown that for an appropriate choice of nonlinear scaling fields, these data also scale, with a scaling function in good agreement with our previous results.

Next, in Section 4, we calculate the scaling behavior of the average volume of vesicles of fixed surface area to leading order in $1/\kappa$. It is found that there is a weak breakdown of scaling, and that instead of $\langle V \rangle / V_0$, it is the quantity

$$[\langle V \rangle - V_0]/V_0 + \frac{1}{2} \ln(4\pi\kappa/3) , \tag{8}$$

where V_0 is the volume of a spherical vesicle with the prescribed surface area, that scales. Reanalyzing our data using (8), we find that there is an excellent collapse of all of our large-κ data. Furthermore, our resulting scaling function is in good agreement with the analytic result derived here for the large-κ regime. For smaller κ, however, the scaling it somewhat worse. Possible causes for this behavior are discussed. The paper closes in Section 5 with a brief discussion of the implications of these results and a short discussion of reasonable choices for discretized bending energies.

2. Bending Energy Discretizations

A general introduction to methods for discretizing operators on triangulated random surfaces is given in reference [19]. For a scalar field ϕ_i defined on the nodes of the lattice, the Laplacian $(-\Delta\phi)_i$ can be written as

$$(-\Delta\phi)_i = \frac{1}{\sigma_i} \sum_{j(i)} \frac{\sigma_{ij}}{l_{ij}} (\phi_i - \phi_j) , \tag{9}$$

where the sum is over the neighbors of site i. l_{ij} is the distance between the two nodes i and j, σ_{ij} is the length of a bond in the dual lattice [19], and

$$\sigma_i = \frac{1}{4} \sum_{j(i)} \sigma_{ij} l_{ij} \tag{10}$$

is the area of the virtual dual cell of vertex i. The length σ_{ij} in equations (9, 10) is given by $\sigma_{ij} = l_{ij}[\cot(\theta_1) + \cot(\theta_2)]/2$, where θ_1 and θ_2 are the two angles opposite link ij in the triangles (ijk) and (ijk'), respectively. Note that since $\cot(\theta) < 0$ if θ is obtuse, σ_{ij}/l_{ij} can be negative if the sides of the two triangles are significantly different. Although there are some sum rules, such as $\sum_i \sigma_i = A$, where A is the area of the surface, there is no guarantee, in general, that the σ_{ij}, or even the σ_i, are positive [19].

Using expressions (9) and (10), the bending energy

$$\beta\mathcal{H}^{\mathrm{Lap}} = \frac{\kappa}{2}\int \mathrm{d}S\ (\Delta\mathbf{R})^2 \tag{11}$$

can be written as [19,22]

$$\beta\mathcal{H}_{\mathrm{d}}^{\mathrm{Lap}} = \frac{\tau}{2}\sum_i \sigma_i(\Delta\mathbf{R})_i^2 = \frac{\tau}{2}\sum_i \frac{1}{\sigma_i}\left[\sum_{j(i)} \frac{\sigma_{ij}}{l_{ij}}(\mathbf{R}_i - \mathbf{R}_j)\right]^2 , \tag{12}$$

with

$$\tau = \kappa. \tag{13}$$

The bending energy can also be expressed in terms of the gradient of the unit normal vector field $\mathbf{n}$ as [23]

$$\beta\mathcal{H}^{\mathrm{n}} = \frac{\kappa}{2}\int \mathrm{d}S\ \partial^i\mathbf{n}\cdot\partial_i\mathbf{n} \equiv \frac{\kappa}{2}\int \mathrm{d}S\ (H^2 - 2K)\ . \tag{14}$$

For surfaces of fixed topology, the contribution from the Gaussian curvature is a constant which can be ignored. On a discretized surface, it is natural to express (14) in terms of the unit normals of the elementary triangles. In this case, equation (14) can be written as [19]

$$\beta\mathcal{H}_{\mathrm{d}}^{\mathrm{n}} = \frac{\kappa}{2}\sum_{\langle i,j\rangle} \frac{l_{ij}}{\sigma_{ij}}(\mathbf{n}_{ijk} - \mathbf{n}_{ijk'})^2 , \tag{15}$$

where (ijk) and (ijk') are the two triangles adjacent to the link ij with compatible orientations, and the sum runs over all links ij.

As noted in the previous paragraph, there is no guarantee that the σ_{ij}, or even the σ_i, are positive. In simulations of self-intersecting random surfaces, the shape and size of the surface triangulations fluctuate wildly, and this can be a significant problem [22,24]. However, because of the way we ensure self-avoidance (see Sect. 3), the angles θ can never exceed 104° for the longest tether lengths we employ, so that although the σ_{ij} are occasionally negative, (12) still provides an accurate discretization of the bending energy. On the other hand, since one *divides* by σ_{ij} in (15), $\beta\mathcal{H}_{\mathrm{d}}^{\mathrm{n}}$ is a very unstable discretization, and, if some σ_{ij} is small enough, the contribution from a single link can dominate the bending energy. For this reason, one often makes the approximation that all surface triangles are equilateral [18,23], so that $\sigma_{ij} = l_{ij}/\sqrt{3}$. In this case, equation (15) reduces to

$$\beta\mathcal{H}_{\mathrm{d}}^{\mathrm{nn}} = \frac{\lambda}{2}\sum_{\langle\alpha,\beta\rangle} (\mathbf{n}_\alpha - \mathbf{n}_\beta)^2 \equiv \lambda\sum_{\langle\alpha,\beta\rangle} (1 - \mathbf{n}_\alpha\cdot\mathbf{n}_\beta)\,, \tag{16}$$

with

$$\lambda = \sqrt{3}\kappa\ , \tag{17}$$

where $\mathbf{n}_\alpha$ is the unit normal vector of triangle α, and the sum runs over all pairs of neighboring triangles. This form of the bending energy is often employed in simulations [18]. However,

there has been some disagreement concerning the relationship between the coupling constant λ in (16) and the bending rigidity κ. Whereas it has been argued that relation (17) is obtained for a spherical vesicle [10], a straightforward calculation yields $\lambda = 2\kappa/\sqrt{3}$ for a cylinder [23,25,26]. This discrepancy, which does not seem to have been appreciated until now, can have important consequences when simulation results are compared with theory. In particular, the effective bending rigidity in equation (16) depends on the membrane shape.

In order to illustrate this effect, we evaluate $\beta\mathcal{H}_{\rm d}^{\rm nn}$ and $\beta\mathcal{H}_{\rm d}^{\rm Lap}$ by covering a sphere and a cylinder with a number N_Δ of equilateral triangles and taking the limit $N_\Delta \to \infty$. In the case of a sphere, we find

$$\beta\mathcal{H}_{\rm d}^{\rm Lap} \approx 8\pi\tau \left\{ 1 - \frac{10\pi}{3\sqrt{3}N_\Delta} + O(1/N_\Delta^2) \right\} \tag{18}$$

and

$$\beta\mathcal{H}_{\rm d}^{\rm nn} \approx \frac{4\pi\lambda}{\sqrt{3}} \left\{ 1 + \frac{2\pi}{3\sqrt{3}N_\Delta} + O(1/N_\Delta^2) \right\} , \tag{19}$$

while for an infinitely long cylinder of unit radius, we have

$$\beta\mathcal{H}_{\rm d}^{\rm Lap} \approx \pi\tau \left\{ 1 - \frac{\pi}{4\sqrt{3}N_\Delta} + O(1/N_\Delta^2) \right\} \tag{20}$$

and

$$\beta\mathcal{H}_{\rm d}^{\rm nn} \approx \frac{\sqrt{3}\pi\lambda}{2} \left\{ 1 - \frac{\pi}{4\sqrt{3}N_\Delta} + O(1/N_\Delta^2) \right\} , \tag{21}$$

per unit length. Since $\beta\mathcal{H}^{\rm n} = \beta\mathcal{H}^{\rm Lap} - 4\pi\kappa(1-g)$, and $g = 0$ for a sphere and $g = 1$ for a cylinder, we see that equations (18, 19) agree in the $N_\Delta \to \infty$ limit if $\lambda = \sqrt{3}\tau = \sqrt{3}\kappa$, while we need $\lambda = 2\tau/\sqrt{3} = 2\kappa/\sqrt{3}$ if (20) and (21) are to be consistent. Note that for a cylinder, the leading finite size corrections to $\beta\mathcal{H}_{\rm d}^{\rm Lap}$ and $\beta\mathcal{H}_{\rm d}^{\rm nn}$ are the same.

Some insight into the origin of this difficulty can be gained by considering a surface consisting of two flat pieces smoothly connected by a cylindrical segment. Let the radius of curvature of the cylindrical region be r_0, and assume that the angle θ between the two flat regions is fixed. The curvature is concentrated in the creased region. The integrated mean curvature for a crease of length l_r is just θl_r, *independent* of the radius of curvature r_0. It is therefore continuous in the limit $r_0 \to 0$; furthermore, it is additive. The resulting curvature remains the same if more creases are added, as long as the subtended angle θ remains fixed. A similar reasoning can be applied to an arbitrary triangulated surface since the curvature is concentrated in the creases in the $r_0 \to 0$ limit. In contrast, it is easy to see that the bending energy (14) is singular in this limit. There is no natural generalization of this operator on triangulated surfaces. More formally, the integrated mean curvature is a Minkowski functional and is additive and continuous [27, 28]. The total bending energy, on the other hand, is not. One way around this problem is to define the discretized bending energy in terms of the square of a local mean curvature. Indeed, (12) is of this form since (twice) the mean curvature at node i is

$$H = \mathbf{n} \cdot \Delta\mathbf{R} \to H_i = \frac{1}{\sigma_i}\mathbf{n}_i \cdot \sum_{j(i)} \frac{\sigma_{ij}}{l_{ij}} (\mathbf{R}_i - \mathbf{R}_j) , \tag{22}$$

where $\mathbf{n}_i$ is the surface normal and σ_i the area associated with node i. Since $\mathbf{n} \parallel \Delta\mathbf{R}$ for surfaces embedded in three dimensions, (22) implies that $\beta\mathcal{H}_{\rm d}^{\rm Lap} = (\tau/2)\sum_i \sigma_i H_i^2$, in agreement with (12). Other discretizations of the bending energy which involve similar local averages of the mean curvature have been used in references [20,21].

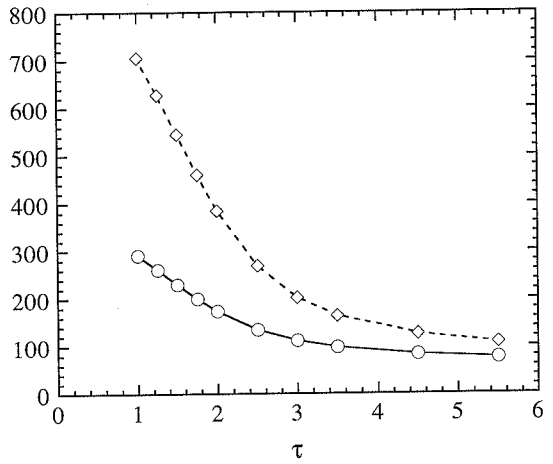

Fig. 1. — $\langle E_{\rm d}^{\rm Lap}\rangle_{\rm Lap}$ (○) and $\langle E_{\rm d}^{\rm nn}\rangle_{\rm Lap}$ (◇) as a function of τ. The averages are taken over configurations generated using $\beta\mathcal{H}_{\rm d}^{\rm Lap}$ and measure (7).

Another way of seeing that the relation between the rigidity parameters λ and τ appearing in the bending energy discretizations is quite complicated is to compare the various approximations for the thermal averages $\langle E\rangle \equiv \langle \int {\rm d}S\ H^2\rangle$ as a function of the bending rigidity. In Figure 1 we have plotted $\langle E_{\rm d}^{\rm Lap}\rangle_{\rm Lap} = \langle \sum_i [\sum_{j(i)} \sigma_{ij}(\mathbf{R}_i - \mathbf{R}_j)/l_{ij}]^2/\sigma_i\rangle_{\rm Lap}$, and $\langle E_{\rm d}^{\rm nn}\rangle_{\rm Lap} = \sqrt{3}\langle \sum_{\langle\alpha,\beta\rangle}(\mathbf{n}_\alpha - \mathbf{n}_\beta)^2\rangle_{\rm Lap} + 8\pi$ *vs.* τ, where averages are taken over a series of configurations generated using $\beta\mathcal{H}_{\rm d}^{\rm Lap}$ and measure (7). It can be seen from equations (18-21) that these two expressions equal 16π in the spherical limit.

Note that $\langle E_{\rm d}^{\rm Lap}\rangle_{\rm Lap}$ is always significantly smaller than $\langle E_{\rm d}^{\rm nn}\rangle_{\rm Lap}$. In fact, surfaces generated using (12) are much rougher on short length scales. The reason for this is that local averages of the curvature are used to determine $\beta\mathcal{H}_{\rm d}^{\rm Lap}$; this averages out a certain amount of roughness on the scale of the nearest-neighbor distance. The difference between these two approximations for the bending energy increases with decreasing τ. We will return to this problem in the next section.

3. Monte Carlo Simulations and the Renormalization of the Bending Rigidity

The model we study consists of N hard spheres of diameter $\sigma = 1$ which are connected by flexible tethers of length $\ell_0 < \sqrt{3}$ to form a two-dimensional network of spherical topology. ℓ_0 is chosen to ensure self-avoidance. In our simulations, we have used $\ell_0 = \sqrt{2.8}$. In order to allow for diffusion within the membrane, and thus to describe fluid membranes, tethers can be cut and reattached between the four beads which form two neighboring triangles [29–32]. A Monte Carlo step (MCS) then consists of an attempt to update the positions of all N beads by a random increment in the cube $[-s, s]^3$, followed by N attempted tether cuts. We chose $s = 0.15$ so that approximately 50% of the attempted coordinate updates were successful. Averages were typically calculated over runs from 20 to 100 million MCS.

In our previous simulations [9], we employed the bending energy (16) using $\lambda = \sqrt{3}\kappa$, and measure (6). A complete discussion of the phase diagram and scaling behavior of this model as a function of κ and the pressure increment Δp has been presented in reference [9]. The scaling behavior of the average volume $\langle V\rangle$ of flaccid fluid vesicles as a function of the bare bending rigidity κ was also analyzed in that paper using a simple scaling ansatz. In analogy

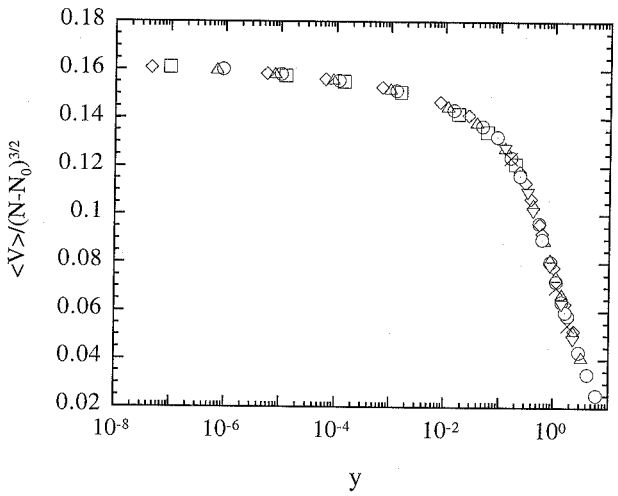

Fig. 2. — The scaled volume $\langle V\rangle/(N-N_0)^{3/2}$ as a function of the scaling variable $y = \sqrt{N}/\xi = \sqrt{N}\exp(-4\pi\lambda/3\sqrt{3})$ for $0.5 \leq \lambda \leq 8$, using $N_0 = 0.8$. The data were obtained using bending energy (16) and $\ell_0 = \sqrt{2.8}$. The plot contains data obtained with measure (6) and $N = 127$ ($\diamond$), $N = 247$ ($\triangle$), $N = 407$ ($\bigcirc$), and $N = 607$ ($\square$), as well as data obtained with measure (7) and $N = 127$ ($\odot$), $N = 247$ ($\triangledown$), and $N = 407$ ($\times$).

with the scaling analysis of ring polymers in two dimensions [33–36], it was argued that the average volume should scale as

$$\langle V\rangle = V_\infty N^{3/2}\Theta_V(y) \tag{23}$$

where y is the ratio of the two relevant length scales in the problem, the radius $R_{\rm ves} \sim \sqrt{N}$ of the large-κ vesicle and the persistence length [5–7]

$$\xi_{\rm p} = a_0(\ell_0)\ \exp\left(\frac{4\pi}{3}\kappa\right)\ . \tag{24}$$

$a_0(\ell_0)$ is a non-universal length scale which depends on the tether length, interaction potential, *etc.* If scaling is complete, the scaling function should describe the behavior of branched-polymer-like vesicles, where $\langle V\rangle \sim N$, in the limit $y \to \infty$. We therefore expect

$$\Theta_V(y) \sim y^{-1} \tag{25}$$

for large y.

In our simulations, the most significant finite-size effects occur in the determination of the prefactor $N^{3/2}$ in equation (23). In order to incorporate the leading finite-size effects, we introduce a "shift" parameter N_0 and replace N by $N - N_0$ when determining the scaled volume. Similar procedures have been employed, for example, in references [34,36]. In Figure 2, $\langle V\rangle/(N-N_0)^{3/2}$ is plotted as a function of $\sqrt{N}/\xi$ for $0.5 \leq \lambda \leq 8$, where $\xi = \exp[4\pi\lambda/3\sqrt{3}]$ is the dimensionless persistence length. The data were obtained using bending energy (16) and measure (6). We have used $N_0 = 0.8$ when plotting the data. This plot contains the data already presented in reference [9], together with new data for $\lambda > 2.5$. As can be seen, the scaling is excellent. Furthermore, the quality of the data collapse for small λ indicates that the linear renormalization group result (2) remains valid in this entire regime ($\lambda > 0.5$). Higher order corrections (in $1/\kappa$) become important only for $\lambda < 0.5$ [37]. Data obtained using the

naive measure (7), which are also included in the figure, are in good agreement with the data obtained using measure (6). We have also checked the quality of the data collapse for other values of the exponential prefactor in the persistence length. If we use the parameterization $\xi = \exp[\beta_\lambda \lambda/\sqrt{3}]$, we find that data collapses of similar quality are obtained for $3.4 \leq \beta_\lambda \leq 4.4$.

There is a simple argument which indicates why the scaling behavior of $\langle V \rangle$ is the same for the two measures (6) and (7). First, write

$$\prod_i (q_i/3)^{3/2} = \exp[(3/2)\sum_i \ln(q_i/3)] \; . \tag{26}$$

Since $\sum_i q_i = 2N_b = 6(N-2)$ for a vesicle, where N_b is the number of bonds, set $q_i = 6 + \epsilon_i$. It follows that

$$\begin{aligned} \sum_i \ln(q_i/3) &= \sum_i \ln(2 + \epsilon_i/3) \\ &= N\ln(2) + \sum_i \ln(1 + \epsilon_i/6) \\ &= N\ln(2) + (1/6)\sum_i \epsilon_i - (1/2)\sum_i (\epsilon_i/6)^2 + \cdots \\ &= N\ln(2) - 12/6 - (1/2)\sum_i (\epsilon_i/6)^2 + \cdots . \end{aligned} \tag{27}$$

On the other hand, the surface triangles are all Euclidean; if we denote by θ_i the sum of the internal angles at vertex i, the Euler characteristic of the triangulated surface can be written as [19]

$$\chi = \sum_i \left(1 - \frac{\theta_i}{2\pi}\right) , \tag{28}$$

where the sum runs over the lattice nodes. Since $\int \mathrm{d}S \; K \to \sum_i \sigma_i K_i$, we have $\sigma_i K_i = 2\pi - \theta_i$. If we further assume, as in reference [30], that all triangles are equilateral (and have area A_Δ), $\sigma_i = q_i A_\Delta/3$ and $\theta_i = 2\pi q_i/6$, so that $A_\Delta K_i = -\pi\epsilon_i/3q_i$. It follows that $\sum_i \epsilon_i^2 \sim \int \mathrm{d}S \; K^2$ so that the term $\prod_i (q_i/3)^{3/2}$ in the measure (6) contributes only terms of higher order than the bending energy to the Hamiltonian. These terms should therefore scale to zero at large distances and not change the scaling behavior. As argued in reference [30], we do not expect that the assumption that the surface triangles are equilateral and have a fixed area will change the scaling behavior, so that this result should also apply to the current model.

The results of a similar analysis of data obtained using the discrete Laplacian bending energy (12) and measure (7) are shown in Figure 3a. We have used $\xi = \exp[\beta_\tau \tau]$, with $\beta_\tau = 4\pi/3$, and $N_0 = 3$; data are presented for $1 \leq \tau \leq 5.5$. While the large-τ data scale quite well, it can be seen that there is a rather strong breakdown of scaling for smaller values of τ. This is surprising, since the data are all in the τ-range where our data obtained using bending energy (16) scaled. This suggests that, as in the case of polymer rings in two-dimensions [36], τ is not the appropriate scaling field in the small-τ regime. In general, there is no reason to expect that the linear relation between the coupling constant of any discretization of the bending energy and the bending rigidity, which is obtained for large κ, extends to the low-bending-rigidity regime. Both the non-linearities of the bending-energy discretization, as well as the direct interactions between the vertices — given by the tethers and hard spheres — contribute to this relation. Indeed, we find an excellent collapse of our data if we utilize the nonlinear scaling field

$$\kappa_{\mathrm{eff}}(\tau) = \frac{0.85 + \tau^2}{3 + \tau} \tag{29}$$

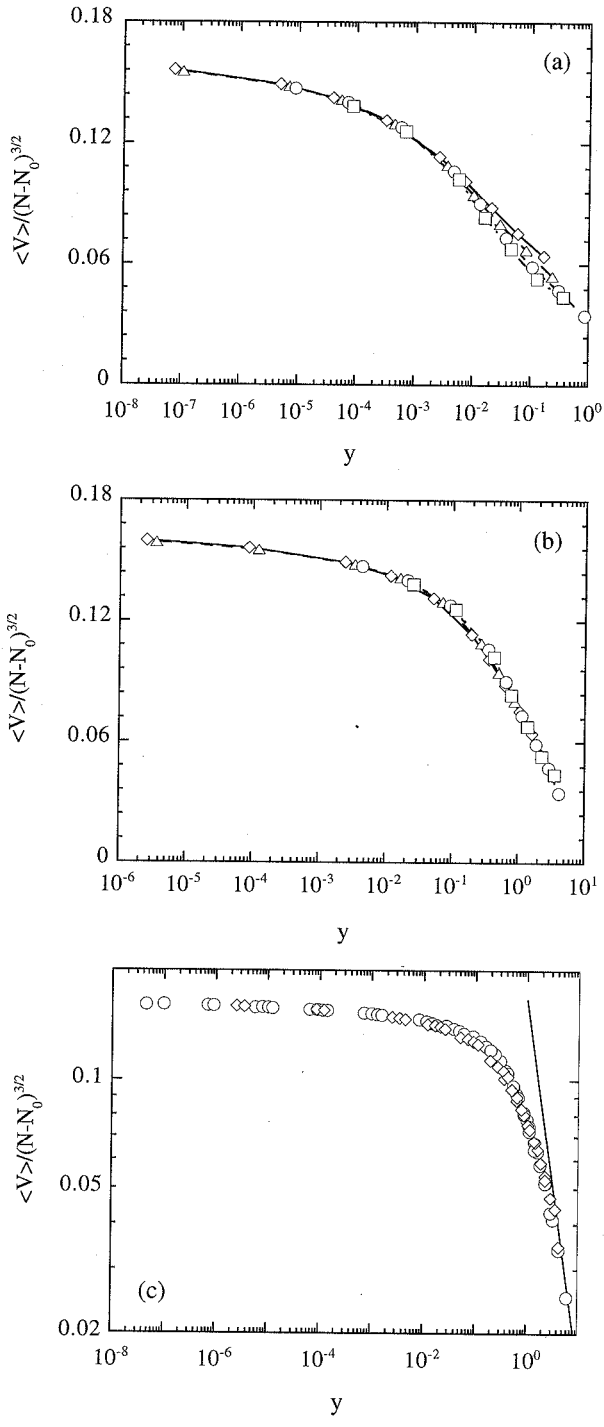

Fig. 3. — (a) The scaled volume $\langle V\rangle/(N-N_0)^{3/2}$ as a function of the scaling variable $y = \sqrt{N}/\xi$, with $\xi = \exp(4\pi\tau/3)$, for $1 \leq \tau \leq 5.5$, using $N_0 = 3$. The data were obtained using bending energy (12), $\ell_0 = \sqrt{2.8}$, and measure (7). Data for $N = 127$ ($\diamond$), $N = 247$ ($\triangle$), $N = 407$ ($\bigcirc$), and $N = 607$ ($\square$) are plotted. (b) The same data plotted as a function of $y = \sqrt{N}/\exp[4\pi\kappa_{\rm eff}(\tau)/3]$. (c) Comparison of data plotted in Figure 2 ($\bigcirc$) with that of Figure 3b ($\diamond$). The solid line is proportional to $\xi/\sqrt{N}$.

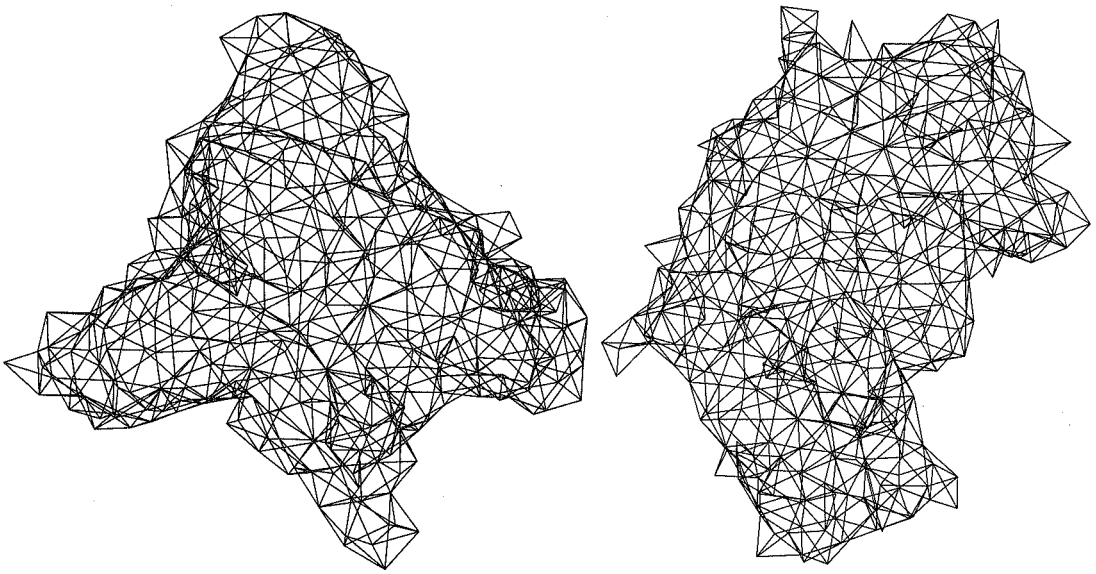

a) b)

Fig. 4. — Typical configurations of thermally fluctuating fluid vesicles obtained in simulations using (a) bending energy (16) for $\lambda = 1.1$, and (b) Laplacian bending energy (12) for $\tau = 1.5$. Note that in (a), equation (17) implies that $\kappa_{\rm eff}(\lambda) = \lambda/\sqrt{3} \simeq 0.64$, while in (b), equation (29) implies $\kappa_{\rm eff}(\tau) \simeq 0.69$; the effective bending rigidities are therefore approximately the same in both cases.

instead of τ in our analysis. The resulting scaling function is shown in Figure 3b; the results presented in Figures 2 and 3b are plotted together in Figure 3c for comparison. It can be seen that the agreement is excellent. The small differences in the shoulder region, for $\sqrt{N}/\xi \approx 0.1$, could probably be removed by some fine tuning of the nonlinear scaling field. The solid line in Figure 3c is the expected large-y scaling behavior $\Theta_V(y) \sim y^{-1}$.

Asymptotically, for large τ, equation (29) reduces to the shift $\kappa_{\rm eff}(\tau) \sim \tau - 3$, while for $\tau \to 0$, $\kappa_{\rm eff}(\tau)$ approaches 0.28. As in the case of polymers, it appears that the peeling off of the small-τ data in Figure 3a is due to a saturation of $\kappa_{\rm eff}(\tau)$ for $\tau \to 0$ caused by the finite thickness and local self-avoidance constraints of our model membrane [38]. The shift contained in equation (29) for large τ is consistent with the increased roughness of the surfaces we observe in simulations using the discrete Laplacian bending energy, compare Figure 1. It also explains the differences observed [24] in the position of the peak in the specific heat in simulations performed using the discrete-Laplacian bending energy and bending energy (16). A comparison of configurations obtained using the discretizations (12) and (16) with approximately the same effective bending rigidities $\kappa_{\rm eff}(\tau)$ and $\kappa_{\rm eff}(\lambda) \equiv \lambda/\sqrt{3}$ is shown in Figure 4.

4. Scaling Behavior of the Average Volume

To go beyond the scaling ansatz (23), we calculate the scaling behavior of the average volume of a nearly spherical vesicle in this section to leading order in the large bending-rigidity limit. In particular, we show that $\langle V \rangle$ is not a homogeneous function of the persistence length and the vesicle radius, but that there is a weak breakdown of scaling, with a logarithmic correction term of the form $\ln(4\pi\kappa/3)$.

We assume that the vesicle has a fixed surface area $A_0 = 4\pi r_0^2$, where r_0 is the radius of a spherical vesicle in the $\kappa \to \infty$ limit. Expanding about a sphere of radius r_0, the radial position vector of the vesicle at solid angle $\Omega \equiv (\theta, \phi)$ can be written as

$$r(\Omega) = r_0[1 + u(\Omega)] \,, \tag{30}$$

where $u(\Omega)$ is the dimensionless amplitude of radial displacement. An expansion of u in spherical harmonics reads

$$u(\Omega) = \sum_{l=0}^{l_M} \sum_{m=-l}^{l} u_{lm} Y_{lm}(\Omega) \,, \tag{31}$$

where l_M is a large wavenumber cutoff determined by the number of degrees of freedom; since only motion normal to the vesicle surface is relevant, $(l_M + 1)^2 = N$ in the present case. Using equation (31), the excess bending energy $\Delta E \equiv (\kappa/2)[\int \mathrm{d}S\ H^2 - 16\pi]$, area A, and volume V of the vesicle can be written (to order u^2) as [39,40]

$$\Delta E = \frac{\kappa}{2} \sum_{l,m} |u_{lm}|^2 \ l(l+1)(l-1)(l+2) \,, \tag{32}$$

$$A = 4\pi r_0^2 (1 + u_0)^2 + r_0^2 \sum_{l>0} |u_{lm}|^2 \ [1 + l(l+1)/2] \,, \tag{33}$$

and

$$V = \frac{4\pi}{3} r_0^3 (1 + u_0)^3 + r_0^3 \sum_{l>0} |u_{lm}|^2 \,, \tag{34}$$

where $u_0 = u_{00}/(4\pi)^{1/2}$.

The constant area constraint is incorporated by choosing u_0 to satisfy $A = 4\pi r_0^2$. This gives

$$(1 + u_0)^2 = 1 - \frac{1}{4\pi} \sum_{l>0} |u_{lm}|^2 \ [1 + l(l+1)/2] \,. \tag{35}$$

The substitution of this result in equation (34) yields

$$V = \frac{4\pi}{3} r_0^3 + \frac{1}{2} r_0^3 \sum_{l>1} |u_{lm}|^2 [1 - l(l+1)/2] \tag{36}$$

to leading order in u.

Equations (32) and (36) imply that the expectation value of the volume is

$$\langle V \rangle = V_0 \left\{ 1 + \frac{3}{8\pi\kappa} \sum_{l=2}^{l_M} \frac{(2l+1)[1 - l(l+1)/2]}{l(l+1)(l-1)(l+2)} \right\} \,, \tag{37}$$

where $V_0 = 4\pi r_0^3/3$. Approximating the sum in (37) by an integral, we have

$$\langle V \rangle / V_0 \approx 1 - \frac{3}{8\pi\kappa} \int_2^{l_M} \frac{\mathrm{d}l}{l} = 1 - \frac{3}{8\pi\kappa} \ln(l_M/2). \tag{38}$$

Note that $\langle V \rangle / V_0$ does *not* scale in $\xi_p/\sqrt{N}$. In order to gain some insight into the behavior for moderate κ, we incorporate the effect of the scale dependence of κ in an approximate way by replacing κ in (37) by the scale-dependent renormalized bending rigidity

$$\kappa_R(\ell) = \kappa - \frac{3}{4\pi} \ln(\ell/a_0) \,. \tag{39}$$

In terms of l, equation (39) can be written as

$$\kappa_{\rm R}(l) = \kappa - \frac{3}{4\pi}\ln(y_0 l_{\rm M}/l) = \frac{3}{4\pi}\ln(l\xi/y_0 l_{\rm M}) \ , \tag{40}$$

where $\xi = \xi_{\rm P}/a_0$, and y_0 is a non-universal, model-dependent scale factor [41]. Using equation (40) in (37), we finally obtain

$$[\langle V\rangle - V_0]/V_0 = \frac{1}{2}\sum_{l=2}^{l_{\rm M}} \frac{(2l+1)[1-l(l+1)/2]}{\ln(l\xi/y_0 l_{\rm M})\, l(l+1)(l-1)(l+2)} \ . \tag{41}$$

Approximating the sum in (41) by an integral, we have

$$\langle V\rangle/V_0 - 1 \approx -\frac{1}{2}\int_2^{l_{\rm M}} \frac{{\rm d}l}{l\,\ln(l\xi/y_0 l_{\rm M})} = -\frac{1}{2}\ln[\ln(\xi/y_0)] + \frac{1}{2}\ln[\ln(2\xi/y_0 l_{\rm M})]. \tag{42}$$

This implies that there is a weak logarithmic correction to scaling and that

$$\langle V\rangle/V_0 - 1 = -\frac{1}{2}\ln[\ln(\xi/y_0)] + \Omega_V(y) \ , \tag{43}$$

where

$$y = y_0\, l_{\rm M}\, \exp\left(-\frac{4\pi}{3}\kappa\right) \ . \tag{44}$$

To first order in $1/\kappa$, the scaling function is

$$\Omega_V^0(y) = \frac{1}{2}\ln[\ln(2/y)] \ . \tag{45}$$

Note that the scaling function $\Omega_V^0(y)$ becomes singular for $y \nearrow 2$, *i.e.* when the persistence length becomes on the order of the system size. This is an artifact caused by using the linear renormalization group result (40) in the limit in which the renormalized bending rigidity goes to zero.

5. Analysis of Monte Carlo Data

Taking equation (43) as a guide, we have reanalyzed our data for the average volume $\langle V\rangle$. The results of a scaling analysis of the data obtained using both the bending energy (16) and measure (6) as well as the discrete Laplacian bending energy (12) and measure (7) (with the nonlinear scaling field $\kappa_{\rm eff}(\tau)$) are shown in Figure 5a. We have used the same persistence lengths ξ and shift factors N_0 as in Figures 2 and 3b, as well as $y_0 = 1$. V_0 was determined for the four system sizes studied using result (37) in the large bending rigidity regime. Data obtained for bending rigidities as large as 80 are included in the figure. The solid line is a plot of the predicted scaling function (45). There are no adjustable parameters. The quality of the agreement between the data and the scaling function $\Omega_V^0(y)$ lends strong support to the prediction that $\langle V\rangle/V_0 + \frac{1}{2}\ln[\ln(\xi)]$, with $\xi = \exp[4\pi\kappa/3]$, scales in $\sqrt{N}/\xi_{\rm P}$ in the large-κ regime.

In order to better illustrate the quality of the scaling behavior for moderate values of κ (with $-10 < \ln(y) < 2$), we have replotted data obtained using bending energy (16) in Figure 5b [42] and that obtained using bending energy (12) in Figure 5c. It can be seen that the data collapse is not perfect for $\ln(y) \geq -4$. There are several possible explanations for this. First, the form

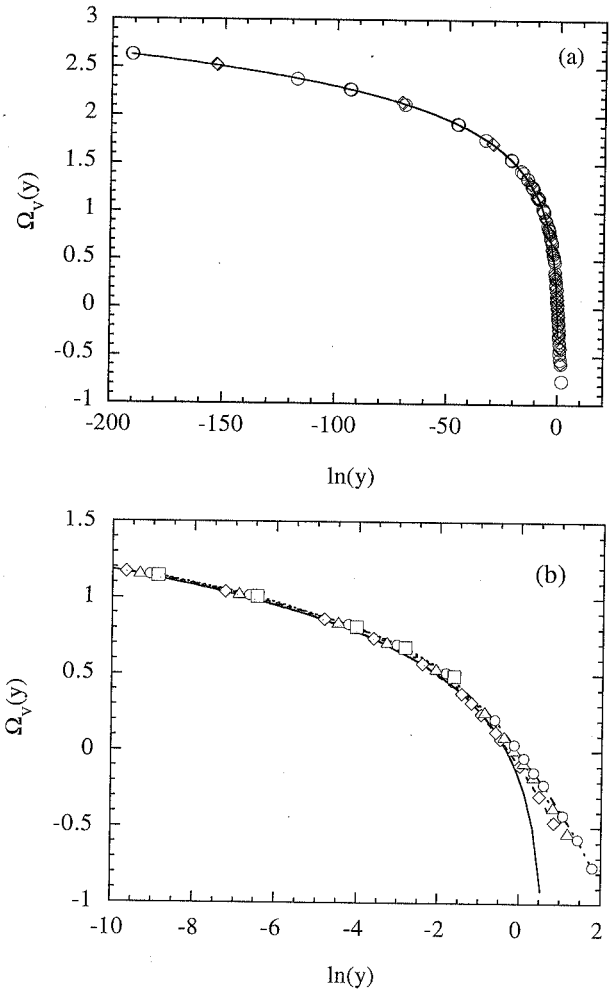

Fig. 5.— Scaling function $\Omega_V(y)$ for the average volume as a function of the ratio of the vesicle radius and persistence length. (a) $\Omega_V(y) = \langle V\rangle/V_0 - 1 + \frac{1}{2}\ln[4\pi\kappa_{\rm eff}(\tau)/3]$ *vs.* $y = \sqrt{N}/\exp[4\pi\kappa_{\rm eff}(\tau)/3]$ ($\diamond$). Data for $1 \leq \tau \leq 40$ were obtained using bending energy (12), $\ell_0 = \sqrt{2.8}$, and measure (7). $\Omega_V(y) = \langle V\rangle/V_0 - 1 + \frac{1}{2}\ln(4\pi\lambda/3\sqrt{3})$ *vs.* $y = \sqrt{N}/\exp[4\pi\lambda/3\sqrt{3}]$ ($\bigcirc$). Data for $0.65 \leq \lambda \leq 80$ were obtained using bending energy (16), $\ell_0 = \sqrt{2.8}$, and measure (6). The solid line is a plot of $\Omega_V^0(y) = \frac{1}{2}\ln[\ln(2/y)]$. (b) $\Omega_V(y) = \langle V\rangle/V_0 - 1 + \frac{1}{2}\ln[\ln(\xi)]$ *vs.* $y = \sqrt{N}/\xi$, with $\xi = \exp[4\pi\lambda/3\sqrt{3}]$, for data obtained using bending energy (16), $\ell_0 = \sqrt{2.8}$, and measure (6). Data for $N = 127$ ($\diamond$), $N = 247$ ($\triangle$), $N = 407$ ($\bigcirc$), and $N = 607$ ($\square$) are plotted. The solid line is a plot of $\Omega_V^0(y) = \frac{1}{2}\ln[\ln(2/y)]$. (c) $\Omega_V(y) = \langle V\rangle/V_0 - 1 + \frac{1}{2}\ln[\ln(\xi)]$ *vs.* $y = \sqrt{N}/\xi$, with $\xi = \exp[4\pi\kappa_{\rm eff}(\tau)/3]$, for data obtained using bending energy (12), $\ell_0 = \sqrt{2.8}$, and measure (7). Data for $N = 127$ ($\diamond$), $N = 247$ ($\triangle$), $N = 407$ ($\bigcirc$), and $N = 607$ ($\square$) are plotted. The solid line is a plot of $\Omega_V^0(y) = \frac{1}{2}\ln[\ln(2/y)]$. (d) Comparison of data for $N = 407$ ($\bigcirc$) and $N = 607$ ($\square$) from Figure 5b and data for $N = 407$ ($\times$) and $N = 607$ ($+$) from Figure 5c.

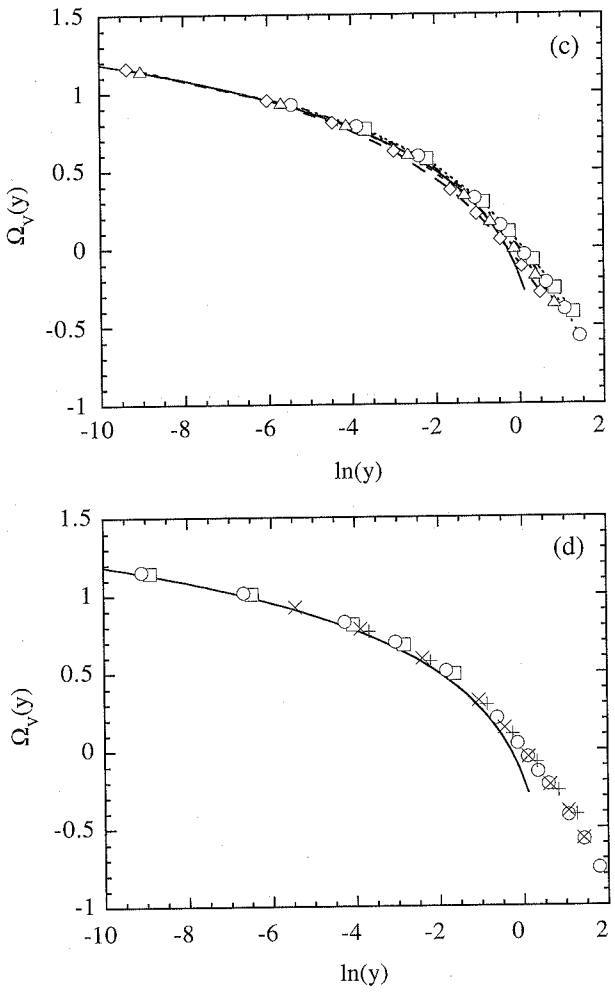

Fig. 5. — *(Continued.)*

of the correction term, $\ln(4\pi\kappa/3)$, is only correct for $\ln(N) \ll 8\pi\kappa/3$, *i.e.* $0 < y \ll 1$. If this condition is not fulfilled, scaling cannot be expected. There also appear to be strong finite size effects. In Figure 5d we have plotted only data obtained for the two largest system sizes studied. While scaling is still not perfect, it is significantly better than that obtained for the smaller sized systems. Small changes in the nonlinear scaling fields could also lead to improved scaling. However, without a better theoretical understanding of the corrections to scaling, it is difficult to resolve these problems given the rather limited range of system sizes which can be studied.

6. Summary and Discussion

The bending energy (16) which is frequently used in simulation studies of both elastic (tethered) surfaces and fluid membranes has the shortcoming that the relationship between the coupling constant λ and the corresponding bending rigidity κ in the Canham-Helfrich bending

energy (1) depends on the membrane shape. While this is not critical problem for qualititative studies, it can lead to difficulties when more quantitative comparisons are made with theory or experiment. Discretizations of the bending energy $\int \mathrm{d}S\ H^2$ based on local averages of discretizations of the mean curvature do not have this shortcoming. One choice, based on the Laplacian-squared representation of the bending energy (12), has been used in this paper to analyze the scaling behavior of the average volume V of flaccid fluid vesicles as a function of the bare bending rigidity and the system size N.

Our Monte Carlo data obtained using bending energy (16) scale just as well as data obtained for the Laplacian bending rigidity. Even in the low-λ regime, where typical configurations are dominated by branched-polymer-like shapes with long, cylindrical arms, we could analyse our data with the same λ-κ relation that is valid for spherical vesicles. On the other hand, since we have only studied vesicles of spherical topology, any shape dependence of the λ-κ relation could always be absorbed in a non-linear scaling field $\kappa_{\mathrm{eff}}(\lambda)$. Our result then simply indicates that $\kappa_{\mathrm{eff}}(\lambda) = \lambda/\sqrt{3}$, with negligibly small non-linear contributions. On the other hand, the shape-dependence of the λ-κ relation certainly leads to problems when the membranes are allowed to change their topology. A transition from many small, spherical vesicles to a few long, cylindrical vesicles, for example, would obviously be affected by this shape dependence.

An explicit calculation in the large-κ limit shows that the average reduced volume $\langle V\rangle/V_0$ is not a homogeneous function of the persistence length ξ_{p} and the vesicle size $R \sim \sqrt{N}$. Rather, there is a weak breakdown of scaling. The correction term was determined in Section 4, and it was shown that the data do indeed scale as predicted in the large-κ regime, with the persistence length $\xi_{\mathrm{p}} \sim \exp[4\pi\kappa/3]$. We have therefore been able to resolve the long-disputed question regarding the universal factor in the exponential κ-dependence of the persistence length in favor of the field-theoretic result [5–7].

The weak breakdown of scaling is not unexpected in view of the fact that the renormalization-group calculations indicate that the theory is asymptotically free. What is needed now is a full field-theoretic calculation of both the correction term and the accompanying scaling function, which takes into account the Fadeev-Popov determinant and the Liouville factor discussed in reference [17]. It would also be of interest to compare the results of a calculation of the specific heat with simulation results. This would allow a more precise comparison of theory and simulation and give further insight into the quality of the operator discretizations.

Acknowledgments

We thank Frank Jülicher and Herbert Wagner for helpful discussions. D.M.K. is grateful for the hospitality of the Max-Planck-Institut für Kolloid- und Grenzflächenforschung during the final stages of writing this manuscript. This work was supported in part by the Deutsche Forschungsgemeinschaft through Sonderforschungsbereich 266, the National Science Foundation under Grant No. DMR-9405824, the donors of The Petroleum Research Fund, administered by the ACS, the University of Minnesota Army High Performance Computing Research Center, U.S. Army Contract DAAL03-89-C-0038, and NATO grant CRG910156.

References

[1] D. Nelson, T. Piran and S. Weinberg Eds., Statistical Mechanics of Membranes and Surfaces (World Scientific, Singapore, 1989).
[2] Lipowsky R., *Nature* **349** (1991) 475.
[3] Canham P.B., *J. Theor. Biol.* **26** (1970) 61.

[4] Helfrich W., *Z. Naturforsch.* **28c** (1973) 693.
[5] Peliti L. and Leibler S., *Phys. Rev. Lett.* **54** (1985) 1690.
[6] Förster D., *Phys. Lett. A* **114** (1986) 115.
[7] Kleinert H., *Phys. Lett. A* **114** (1986) 263.
[8] Helfrich W., *J. Phys. France* **46** (1985) 1263.
[9] Gompper G. and Kroll D.M., *Phys. Rev. E* **51** (1995) 514.
[10] Kroll D.M. and Gompper G., *Science* **255** (1992) 968.
[11] Boal D. and Rao M., *Phys. Rev. A* **45** (1992) R6947.
[12] Kroll D.M. and Gompper G., *Phys. Rev. A* **46** (1992) 3119.
[13] Baillie C.F. and Johnston D.A., *Phys. Lett. B* **283** (1992) 55.
[14] Golubović L., *Phys. Rev. E* **50** (1994) R2419.
[15] Morse D.C., *Phys. Rev. E* **50** (1994) R2423.
[16] Gompper G. and Goos J., *J. Phys. II France* **5** (1995) 621.
[17] Cai W., Lubensky T.C., Nelson P. and Powers T., *J. Phys. II France* **4** (1994) 931.
[18] Kantor Y. and Nelson D.R., *Phys. Rev. Lett.* **58** (1987) 2774; *Phys. Rev. A* **36** (1987) 4020.
[19] Itzykson C., Proceedings of the GIFT Seminar, Jaca 85, J. Abad *et al.* Eds. (World Scientific, Singapore, 1986) pp. 130-188.
[20] Gompper G. and Goos G., *Phys. Rev. E* **50** (1994) 1325.
[21] Jülicher F., PhD thesis (Universität zu Köln, 1994).
[22] Espriu D., *Phys. Lett. B* **194** (1987) 271.
[23] Seung H.S. and Nelson D.R., *Phys. Rev. A* **38** (1988) 1005.
[24] Baillie C.F., Johnston D.A. and Williams R.D., *Nucl. Phys. B* **335** (1990) 469.
[25] Zhang Z., Davis H.T., Maier R.S. and Kroll D.M., *Phys. Rev. B* **52** (1995) 5404.
[26] In the analysis of the asymptotic shape of elastic networks in reference [25] (which used the bending energy (16)), it was necessary to use the relation $\lambda = 2\kappa/\sqrt{3}$ in order to get the correct energy for disclinations. The reason for this is that the networks considered were approximately conical in shape in the regions of high energy density.
[27] Mecke K.R. and Wagner H., *J. Stat. Phys.* **64** (1991) 843.
[28] Likos C.N., Mecke K.R. and Wagner H., *J. Chem. Phys.* **102** (1995) 9350.
[29] Billoire A. and David F., *Nucl. Phys. B* **275** (1986) 617.
[30] Boulatov D.V., Kazakov V.A., Kostov I.K. and Migdal A.A., *Nucl. Phys. B* **275** (1986) 641.
[31] Ho J.-S. and Baumgärtner A., *Europhys. Lett.* **12** (1990) 295.
[32] Baumgärtner A. and Ho J.-S., *Phys. Rev A* **41** (1990) 5747.
[33] Leibler S., Singh R.R.P. and Fisher M.E., *Phys. Rev. Lett.* **59** (1987) 1989.
[34] Camacho C.J. and Fisher M.E., *Phys. Rev. Lett.* **65** (1990) 9.
[35] Maggs A.C., Leibler S., Fisher M.E. and Camacho C.J., *Phys. Rev. A* **42** (1990) 691.
[36] Camacho C.J., Fisher M.E. and Singh R.R.P., *J. Chem. Phys.* **94** (1991) 5693.
[37] Ipsen J.H. and Jeppesen C., *J. Phys. I France* **5** (1995) 1563.
[38] Abraham F.F. and Nelson D.R., *J. Phys. France* **51** (1990) 2653.
[39] Milner S.T. and Safran S.A., *Phys. Rev. A* **36** (1987) 4371.
[40] Helfrich W., *J. Phys. France* **47** (1986) 321.
[41] The dimensionless scale factor $y_0 \approx 1$ is related to the ratio of the prefactor a_0 of the persistence length to the average tether length for the network.
[42] If we use the parameterization $\xi = \exp[\beta_\lambda \lambda/\sqrt{3}]$, we obtain data collapses of similar quality for $3.8 \leq \beta_\lambda \leq 4.7$. However, for $\beta_\lambda \neq 4\pi/3$, values of y_0 different from one are needed in order to obtain agreement with the scaling function (45). For example, for $\beta_\lambda = 4.7$, we need to take $y_0 = 2$.